DAΦNE TECHNICAL NOTE
INFN - LNF, Accelerator Division

Frascati, November 28, 2006
Note: **G-68**

DAΦNE UPGRADE FOR SIDDHARTA RUN

D. Alesini, D. Babusci, M.E. Biagini, R. Boni, M. Boscolo, F. Bossi, B. Buonomo, A. Clozza, G. Delle Monache, G. Di Pirro, A. Drago, A. Gallo, S. Guiducci, M. Incurvati, C. Ligi, F. Marcellini, G. Mazzitelli, C. Milardi, L. Pellegrino, M. Preger, L. Quintieri, P. Raimondi, R. Ricci, U. Rotundo, C. Sanelli, M. Serio, F. Sgamma, B. Spataro, A. Stecchi, A. Stella, S. Tomassini, C. Vaccarezza, M. Zobov, *LNF-INFN*
A. D'Angelo, R. Messi, D. Moricciani, *Rome II University Tor Vergata*
S. Bettoni, *CERN*
I. Koop, E. Levichev, P. Piminov, D. Shatilov, V. Smaluk, *BINP*

1. Introduction

The Siddharta experiment will be ready to be installed in DAΦNE by mid-2007. It seems very feasible to install an Interaction Region (IR) suitable to exploit the "large crossing angle" and "crabbed waist" concepts. This new scheme for luminosity increase in e^+e^- colliders, first presented at the 2nd Frascati Workshop on SuperB-Factory, March 2006 [1] has been extensively studied both analytically and with numerical simulations. A combination of large crossing angle, together with very small transverse beam sizes at the IP, and the "crabbed vertical waist", should in theory give us the possibility of reaching a luminosity of the order of 10^{33} cm^{-2} s^{-1}, with very little modifications of the machine and beam currents similar to those stored during the KLOE run [2]. This scheme does not need very short bunches in the rings (very expensive and difficult) in order to reach very low β-functions and little hourglass effect.

Other improvements to DAΦNE will be the installation of fast stripline kickers, as those foreseen for the ILC damping rings. This should increase the injection efficiency with consequent background reduction and possibly higher beam currents, with a further gain in peak and integrated luminosity.

Wigglers poles will also be modified in order to improve the dynamic aperture, with benefits in beam lifetimes and background.

TiN coating in the positron straight vacuum chambers will hopefully improve the electron cloud instability threshold and should allow us to further increase the current.

This paper reviews the principle of the new collision scheme and presents a summary of the beam-beam and background studies performed in order to estimate the luminosity gain. Moreover a description of the lattice and hardware modifications needed for its implementation is given.

2. The large crossing angle and crab waist concepts

In high luminosity colliders one of the key points is to have very short bunches, since this allows to decrease β_y^* at the IP. This value cannot indeed be much smaller than the bunch-length without incurring in the "hourglass" effect. Moreover high luminosity requires small vertical emittance and large horizontal size and horizontal emittance to minimize the beam-beam effect. Unfortunately for a ring it is relatively easy to achieve small horizontal emittance and horizontal size but it is very hard to shorten the bunch length σ_z.

The recently proposed crabbed waist scheme [1] for beam-beam collisions can substantially increase luminosity since it combines several potentially advantageous ideas.

The first one is the large Piwinski angle: for collisions under a crossing angle θ the luminosity L and the horizontal ξ_x and the vertical ξ_y tune shifts scale as (see for example in [3]).

$$L \propto \frac{N\xi_y}{\beta_y} \tag{1}$$

$$\xi_y \propto \frac{N\sqrt{\beta}_y}{\sigma_x\sqrt{1+\phi^2}} \approx \frac{2N\sqrt{\beta}_y}{\sigma_z\theta} \tag{2}$$

$$\xi_x \propto \frac{N}{\sigma_x^2\left(1+\phi^2\right)} \approx \frac{4N}{\left(\sigma_z\theta\right)^2} \tag{3}$$

Piwinski angle ϕ is defined as:

$$\phi = \frac{\sigma_z}{\sigma_x} tg\left(\frac{\theta}{2}\right) \approx \frac{\sigma_z}{\sigma_x}\frac{\theta}{2} \tag{4}$$

σ_x being the horizontal rms bunch size, σ_z the rms bunch length, N the number of particles per bunch. Here we consider the case of flat beams, small horizontal crossing angle $\theta << 1$ and large Piwinski angle $\phi >> 1$.

The idea of colliding with a large Piwinski angle is not new (see for example in [4]). It has been also proposed for the LHC upgrade [5], to increase the bunch length and the crossing angle. In such a case, if it were possible to increase N proportionally to $\sigma_z\theta$, the vertical tune shift ξ_y would indeed remain constant, while the luminosity would grow proportionally to $\sigma_z\theta$ (see eqs. (1)-(2) above). Moreover, the horizontal tune shift ξ_x drops like $1/\sigma_z\theta$ (eq. (3) above), so that for very large ϕ the beam-beam interaction can be even considered in some sense as one-dimensional since the horizontal footprint size shrinks. However, differently from [4], in the crabbed waist scheme described here Piwinski angle is increased by decreasing the horizontal beam size and increasing the crossing angle. In this way we can gain in luminosity as well, and the horizontal tune shift due to the crossing

angle increases. But what is more important is that the overlap area of colliding bunches is getting smaller proportionally to σ_x/θ. So, if the vertical beta function β_y can be made comparable to the overlap area size:

$$\beta_y \approx \frac{\sigma_x}{\theta} << \sigma_z \tag{5}$$

we can get several advantages:

a) small spot size at the IP, i.e. higher luminosity (see eq. (1)),
b) reduction of the vertical tune shift (see eq. (2))
c) suppression of the vertical synchrobetatron resonances [6].

Besides, there are additional advantages in such a collision scheme: there is no need to decrease the bunch length to increase the luminosity as proposed in standard upgrade plans for B- and Φ-factories [7,8,9]. This will certainly ease the problems of HOM heating, coherent synchrotron radiation of short bunches, excessive power consumption etc. Moreover the problem of parasitic collisions (PC) is automatically solved since with higher crossing angle and smaller horizontal beam size the beams separation at the PC is large in terms of σ_x.

However, large Piwinski angle itself introduces new beam-beam resonances and may strongly limit the maximum achievable tune shifts (see for example in [10]). The "crabbed waist" (CW) transformation enters in the game boosting the luminosity: this is mainly due to the suppression of betatron (and synchrobetatron) resonances usually arising (in collisions without CW) through the vertical motion modulation by the horizontal oscillations [11]. A sketch of how the scheme works is depicted in Fig.1 below.

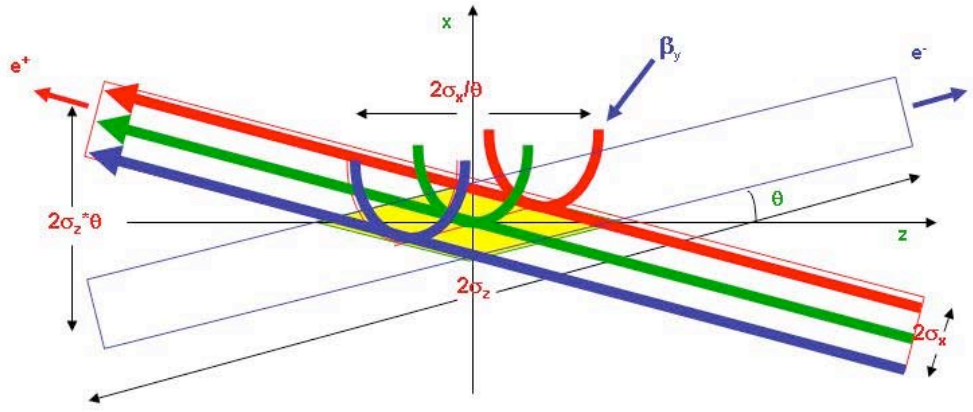

Fig. 1: Large Piwinski angle and crabbed waist scheme. The collision area is in yellow.

The CW correction scheme can easily be realized with a sextupole magnet in phase with the IP in the x plane and at π/2 in the y one, on both sides of the IP, as shown in Fig. 2. In DAΦNE we have sextupoles available for such a scheme, which will only need to be

slightly moved longitudinally. The suppression of sinchrobetatron resonances can be seen in Fig. 5 where a beam-beam tune scan has been performed with and without crabbed waist scheme.

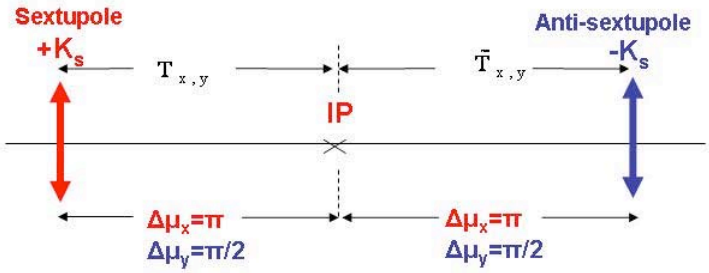

Fig. 2: Crabbed waist correction by sextupole lenses.

3. Beam-beam simulations

In order to estimate the maximum achievable luminosity in the crabbed waist regime and to investigate distribution tails arising from beam-beam collisions, which may affect the beam lifetime, simulations with the numerical codes BBC [12] and LIFETRAC [13] were performed. The beam parameters used for the simulations are summarized in Table I. For comparison, the parameters used during the last DAΦNE run with the KLOE detector (2005-2006) are also shown.

Table I : Comparison of beam parameters for KLOE and Siddharta Runs

	KLOE Run	Siddharta Run
L (cm^{-2} s^{-1})	$1.5x10^{32}$	10^{33}
N_{bunch}	110	110
N_{part}/bunch	$2.65*10^{10}$	$2.65*10^{10}$
I_{bunch} (mA)	13.	13.
ε_x (nm)	300.	200.
ε_y (nm)	1.5	1.
Coupling (%)	0.5	0.5
σ_x (μm)	700.	200.
σ_y (μm)	15.	2.4
σ_z (mm)	25.	20
β_x (m)	1.5	0.2
β_y (mm)	18.	6.
θ (mrad)	2x16	2x25
Crabbed waist factor	-	0.8/ θ

As discussed above, in order to realize the crabbed waist scheme in DAΦNE, Piwinski angle $\phi=\theta\sigma_x/\sigma_z$ should be increased and the beam collision area reduced: this can be achieved by increasing the crossing angle θ by a factor 1.5 and reducing the horizontal beam size σ_x. In this scheme the horizontal emittance ε_x will be reduced by a factor about 1.5, while the horizontal beta function β_x will be lowered from 1.5 to 0.2 m. Since the beam collision length decreases proportionally to σ_x/θ, the vertical beta function β_y can be also reduced by approximately a factor of 3, from 1.8 cm to 0.6 cm. All other parameters will be similar to those already achieved at DAΦNE, in particular the number of bunches, 110, routinely used in collisions.

For what concerns the beam currents, 2 A were reached for the electron beam in collision, whereas a maximum of 1.4 has been reached for the positron beam. We think that this limit can be pushed higher by exploiting new feedback systems [14], installing new injection kickers [15] and with a TiN coating of the straight vacuum chamber. In particular the new feedback systems, which are based on the FPGA (Field Programmable Gate Array) technology, can modify digitally controlled gain and phase response simply through the software interface. This will make the feedback setup faster and more efficient and it will also be possible to manage lower betatron tunes.

At low currents beam coupling at the level of 0.2-0.3% has been achieved in both DAΦNE rings. In collision it increases to about 1.0%, whereas in the crabbed waist scheme it should remain below 0.5%, since there is practically no beam-beam blow-up.

In typical operating conditions the positron bunches are about 2 cm long at 20 mA per bunch. The electron bunches were by 30% longer due to the higher beam coupling impedance of the e- ring, but after the removal, during the 2006 summer shutdown, of the ion clearing electrodes, which contributed to almost half of the impedance budget, we have obtained 2 cm bunch length also in the electron ring.

Using the parameters of Table I and taking into account the finite crossing angle and the hourglass effect luminosity in excess of $1.0\text{x}10^{33}$ cm^{-2} s^{-1} is predicted, with the beam currents stored during the KLOE run, about 6 times higher than the one obtained until now. The only parameter that seems to be most critical for a low energy machine is the high vertical tune shift: ξ_y = 0.08, to be compared with the value of 0.03 so far obtained at DAΦNE. However this tune shift limit should be overcome in the crabbed waist collisions and the beam-beam simulation results presented below not only confirm this, but show that indeed even higher tune shifts and luminosity can be obtained.

Beam-beam simulations have been carried out with the weak-strong code BBC. The code has been successfully used for beam-beam collision studies for the KEK B-factory [16] and DAΦNE [17]. The simulation algorithm is fully symplectic in the 6D phase space, and includes all the known effects as crossing angle, finite bunch length, variation of the beta functions along the bunch, energy loss due to the longitudinal electric fields, etc.

The crabbed waist scheme has been included in a simplified manner: the crabbed waist transformation $y = Kxy'/\theta$ has been applied immediately before the beam-beam interaction and subtracted after the collision. The crabbing sextupole strength variation can be done by changing the parameter K, where K = 1 corresponds to the exact “crabbed” condition.

The working point (0.057, 0.097) has been chosen to start the simulations since it was the best operating point found experimentally at VEPP2M, working at the energy of the Φ-resonance, and also predicted numerically as the best working point for DAΦNE.

The results are shown in Fig. 3, where the green line is the luminosity computed numerically as a function of the single bunch current. It can be seen that the luminosity at a bunch current of 20 mA exceeds already by about 15-20% the value 2.2×10^{33} $cm^{-2}s^{-1}$ calculated using the standard luminosity formula. This is due to the geometrical luminosity gain provided by the crabbed waist scheme. Moreover the luminosity continues to grow for higher bunch currents exceeding the 10^{34} $cm^{-2}s^{-1}$ level at about 50 mA per bunch, scaling quadratically with the bunch current up to 30-35 mA/bunch. This means that the tune shift limit is not reached yet at these currents and it certainly exceeds the design value of 0.08.

Moreover even higher luminosity values can be obtained for smaller horizontal beam size at the IP. The two magenta points in Fig. 3 correspond to a horizontal size by a factor of 2 smaller with respect to the design value of 200 μm.

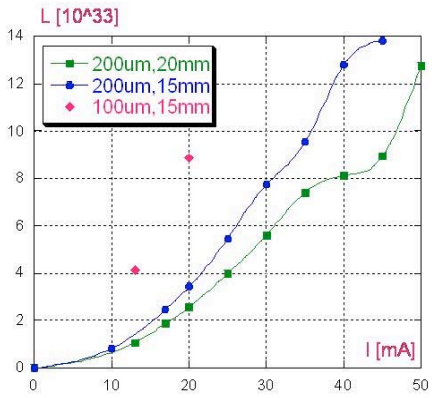

Fig. 3: Luminosity vs bunch current (BBC code). Green line: Siddharta parameters, blue line: shorter bunch length, red dots: smaller horizontal beam size.

Yet another important limitation arising from the beam-beam interaction is the lifetime reduction. The beam-beam collisions create non-Gaussian tails in the transverse beam charge distributions. If the tails reach the physical or dynamic aperture the particles get lost, leading to lifetime degradation. In order to simulate the beam-beam induced tails the numerical code LIFETRAC has been used. The tracking algorithm is essentially similar to that of BBC, however, a special technique used in LIFETRAC allows decreasing, sometimes by several orders of magnitude, the CPU time required to reproduce the charge distribution in the rarely populated beam tails. In the simulations with LIFETRAC the crabbed waist sextupoles have been inserted in an implicit way, as lattice elements satisfying the crabbed waist conditions, i.e. having the strength and betatron phase advances as described in Sec. 2.

Figure 4 shows the beam distribution contour plots in the space of the normalized transverse amplitudes A_x/σ_x and A_y/σ_y. For all the plots the maximum horizontal amplitude A_x is $12\sigma_x$ and the vertical one $160\sigma_y$ (plots scale). The successive contour levels are at a constant ratio of $e^{1/2}$ below each other. The top row of Fig. 4 corresponds to a positive momentum compaction lattice with a normalized synchrotron tune ν_s = 0.01, while the

bottom row represents the simulation results obtained with a negative momentum compaction factor. Each column contains plots for different strengths of the crabbing sextupoles K: K = 1 means the exact crabbed waist condition, for K = 0 the crabbing sextupoles are off.

As can be seen in Fig. 4, a peak luminosity of about 3.0×10^{33} cm^{-2} s^{-1} is achieved both for positive and negative momentum compaction factors. The maximum luminosity is obtained for slightly lower sextupole strengths (K = 0.6-0.8) than required for the "exact" crabbed waist condition, K = 1. The luminosity optimum corresponds also to the shortest distribution tails. With stronger or weaker sextupoles the tails start growing indicating possible lifetime problems.

It is worthwhile to note that even with the crabbing sextupoles off (see the plots with K = 0), a peak luminosity higher than 1.0×10^{33} cm^{-2} s^{-1} can be achieved. Clearly the tails are much longer in this case. However, the lifetime can be improved with dynamic aperture optimization or by using slightly lower bunch currents. It has to be noted that in the KLOE run configuration an increase of the Touschek lifetime was obtained due to coupling increase in collision. In the CW configuration we expect a lifetime reduction of about $\sqrt{2}$. More frequent injections will be needed to keep the integrated luminosity close to the peak value.

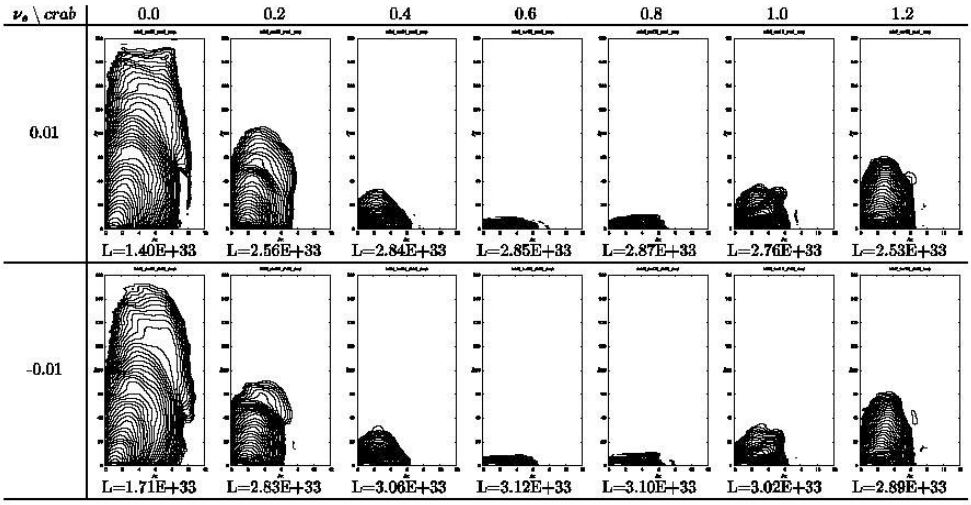

Fig. 4: Luminosity vs crabbing sextupole intensity (LIFETRAC code) for $\alpha_c > 0$ (top row) and $\alpha_c < 0$ (bottom row).

The working point choice is defined not only by the beam-beam interaction, but also by other beam dynamics aspects, such as dynamic aperture, coupling correction etc. For this reason, it is very important to know how large is the good luminosity area in the tune space and where other "safe" working point islands are. To answer to these questions a luminosity vs tunes scan, above the integer tunes in the range Q_x = (0.0, 0.2) and Q_y = (0.0, 0.2) with a tune step of 0.0025 in both directions, has been performed. This tune range is typical for DAΦNE operation and for other low energy machines like VEPP2M, ADONE etc. Figure 5 shows 2D luminosity contour plots for the crabbed waist collisions with K = 0.6 (left) and with the crabbing sextupole off (right). "Geographic map" colors are

used to produce the plots: the brighter red colors correspond to higher luminosities (mountains), while the blue colors are used for the lowest ones (rivers and oceans). For each plot 10 contour lines between the maximum and the minimum luminosities were drawn. Comparing the two plots of Fig. 5 one can deduce that:

a) as expected the good luminosity region with the crabbing sextupoles on is much wider than that with the sextupoles off;
b) many more betatron resonances arise without CW;
c) in the CW collision a high luminosity can be obtained at the working points presently used in DAΦNE, like (0.09, 0.16).

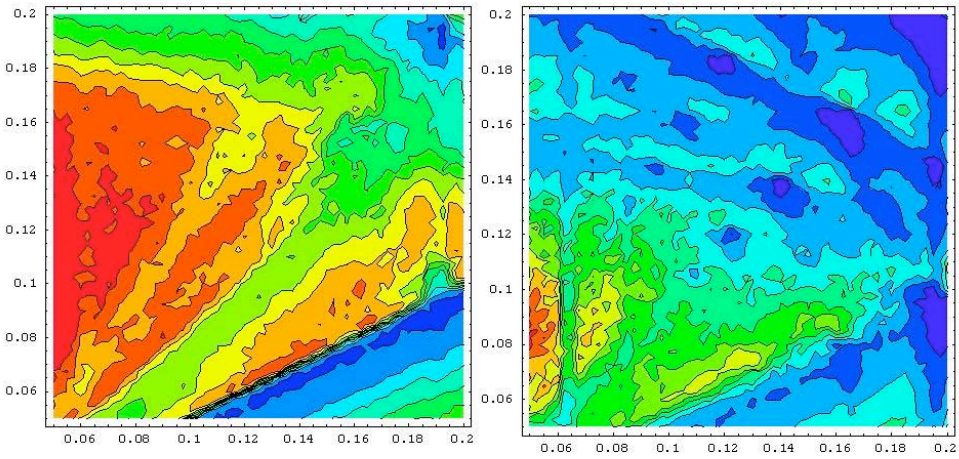

Fig. 5: Luminosity vs tune scan (ν_x=ν_y=0 to 0.2). CW ON, 0.6/θ (left). CW OFF (right).

Moreover, as the plots in Fig. 6 show, the absolute luminosity values are much higher in the crabbed waist collisions: a peak luminosity of 2.97×10^{33} cm^{-2} s^{-1} compares with L_{max} = 1.74×10^{33} cm^{-2} s^{-1} in the case with the crabbing sextupoles off . It should be noted that the worst luminosity value obtained in the crabbed waist collisions, 2.52×10^{32} cm^{-2} s^{-1}, is still higher than the present luminosity record at DAΦNE. With the crabbing sextupoles off the lowest luminosity value drops by an order of magnitude, down to L_{min} = 2.78×10^{31} cm^{-2} s^{-1}.

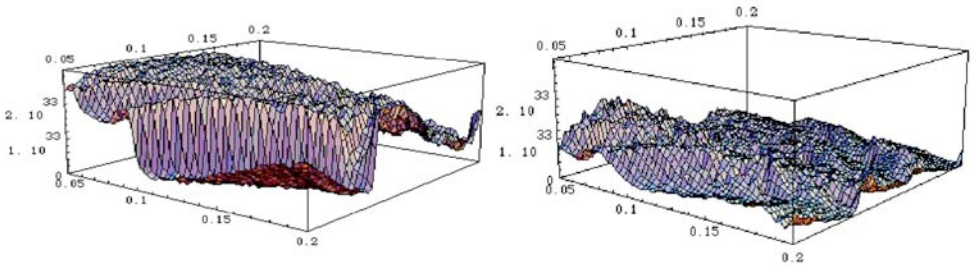

Fig. 6: Luminosity vs tunes. CW ON, 0.6/θ (left). CW OFF (right).

Another possible working point for a collider is the one above half-integer tunes. In particular, the high energy colliders, PEP-II, KEKB and CESR, operate in this tune region. Since there can be some advantages for DAΦNE optics and dynamic aperture optimization in that area, a luminosity scan for tunes between 0.5 and 0.65 has been carried out. The

results are presented in Fig. 7: the picture on the left is the 2D luminosity contour plot, while the one on the right is the 3D plot. In this case a peak luminosity of $3.x10^{33}$ $cm^{-2}s^{-1}$ is numerically achieved. However, the "safe" luminosity area is smaller with respect to the allowable tune space above the integers and it is situated rather close to the half-integer tunes. In order to be sure that a working point above the half-integers can be exploited in DAΦNE one has to check whether an acceptable dynamic aperture can be obtained for these tunes.

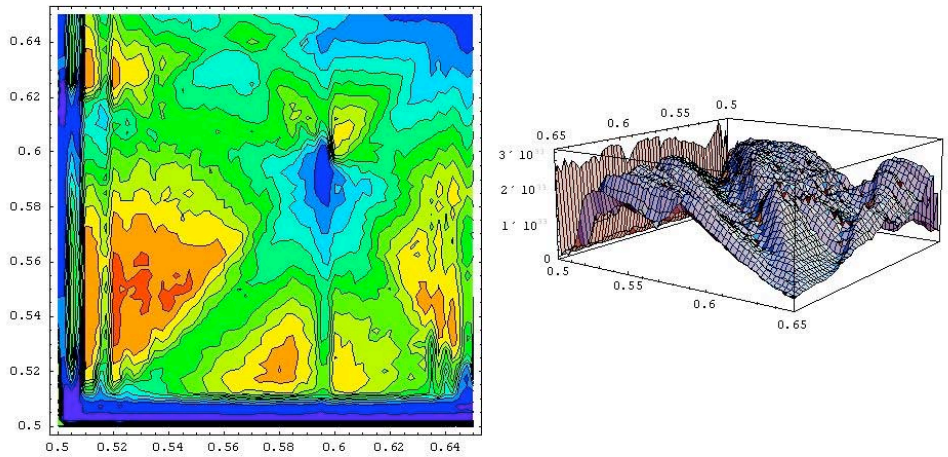

Fig. 7: Luminosity vs tunes above half integer. L_{max} = 3.05 x 10^{33} $cm^{-2}s^{-1}$. L_{min} = 3.28 x 10^{31} $cm^{-2}s^{-1}$.

Another important feature of this scheme is that since there is practically no beam-beam blow up, there is a very weak dependence on the damping time. A simulation with three different damping times, corresponding to the present ones and to those without our very long wigglers, and with very short high field superconducting ones, is shown in Fig. 8, where the vertical beam size blow up (on the left) and the luminosity (on the right) are plotted as a function of the number of turns, for different tune working points.

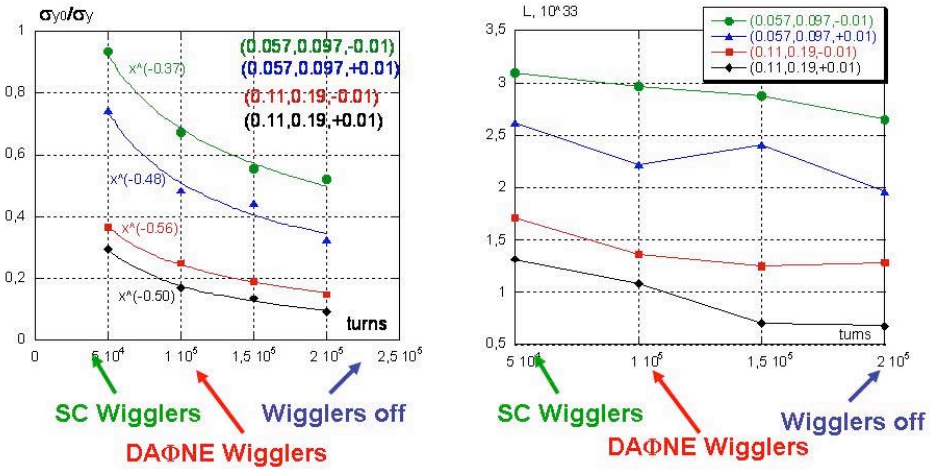

Fig. 8: Vertical beam size ratio (left plot) and luminosity as a function of damping time expressed in number of turns for different tune working points. Arrows show the damping times corresponding to the different wiggler configurations.

4. Interaction Region layout

The need to have a very small β_y* and large crossing angle translates in a new IR geometry. A couple of quadrupoles (QD0s,QF1s) on both sides of the Interaction Point (IP) will provide the necessary focusing at the IP and the needed beam separation. Further trajectory separation will be provided by two small correctors upstream and downstream the doublets. Another three quadrupoles will be used to match the betatron functions to the arcs.

In this solution there will be no need for the two splitter dipoles that are presently used to bring the two beams, traveling together in the IR, to separate beam pipes into the arcs. This is schematically shown in Fig. 9.

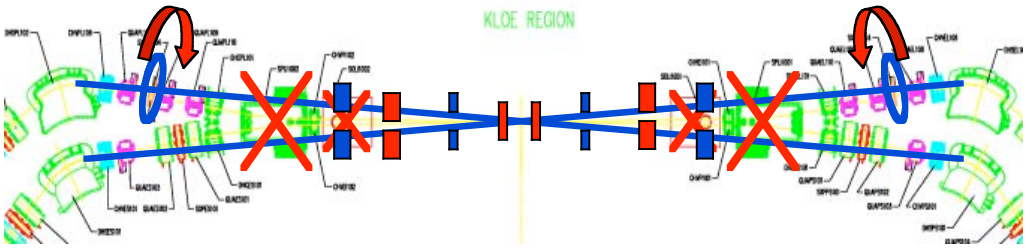

Fig. 9: Sketch of the new IR. In blue are the new beam lines.

The total crossing angle will be 50 mrad (25 mrad per beam), the first quadrupole is 23 cm long, starting at 0.3 m from the IP and its expected deflection is 50 mrad. Beam stay clear will be larger than the present one, due to the smaller beam sizes. Details of the required new hardware are in Sec. 6 and 7.

The lattice has been designed with the IP betatron functions listed in Table I. The betatron functions for the new half IR are shown in Fig. 10, with the "Siddharta" optics beta functions on the left and with the "KLOE" ones on the right. It will be possible indeed to operate with parameters very similar to the ones used for the DEAR and KLOE runs. The matched betatron functions and dispersion in the whole ring are shown in Fig. 11.

A preliminary study of dynamic aperture with the MAD code has given good results, with stable particle with amplitudes larger than 20 σ_x (no coupling) and 12 σ_y (full coupling). Particle trajectories in the (x,x') and (y,y') phase spaces are shown in Fig.12.

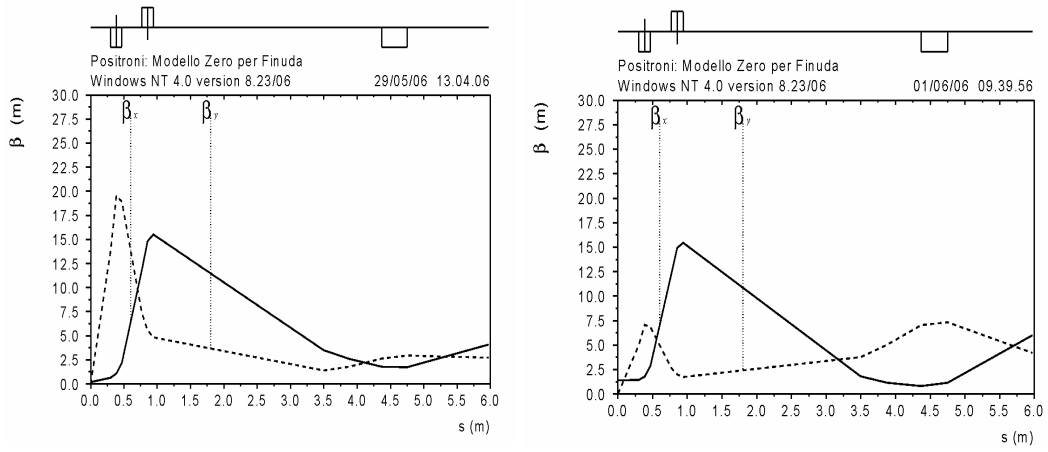

Fig. 10: Half IR betatron functions: Siddharta (left), KLOE (right).

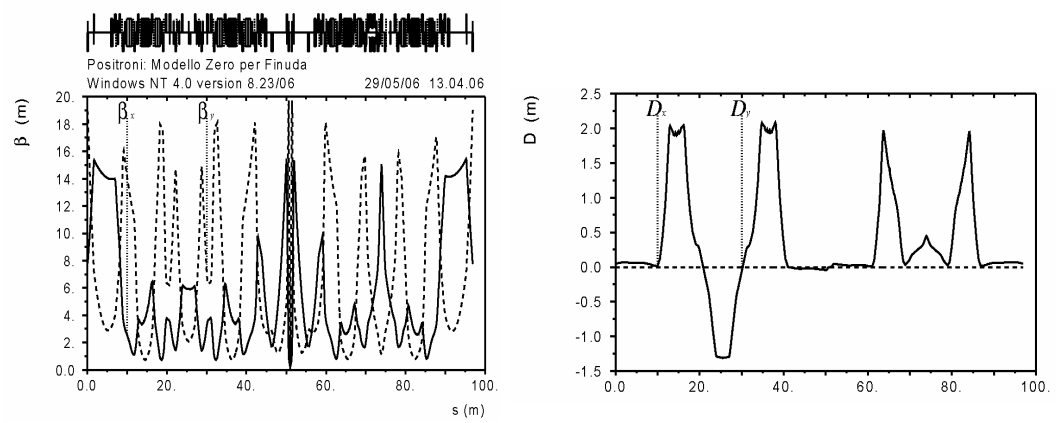

Fig. 11: Ring betatron functions (left) and dispersion (right).

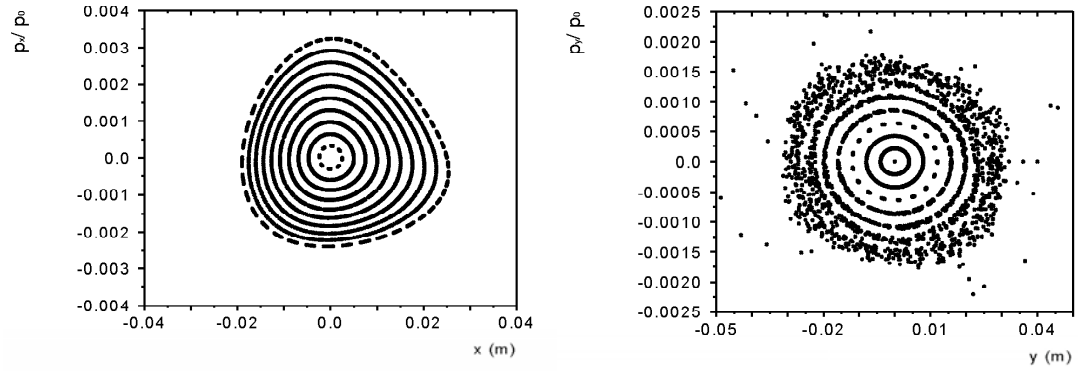

Fig. 12: (x,x') (left) and (y,y') (right) phase space.

5. Wiggler modification

A modification of the DAΦNE wigglers has recently been proposed [18] to improve the nonlinear contributions due to the field roll-off combined with the large amplitude of the beam trajectory inside the wiggler [19]. The idea consists in realizing a magnetic structure symmetric with respect to the quasi-sinusoidal beam trajectory, which in principle contains only even terms in the field expansion around the trajectory itself. Due to the alternating sign of the field in the successive poles and the condition of vanishing field integral along the wiggler, the overall contribution of these even terms tends to vanish, thus leaving the wiggler field almost free from nonlinear terms. Of course this solution offers large advantages for low energy machines with high field wigglers, which is just the case for DAΦNE.

An approximation to the ideal solution of shaping of the poles symmetrically with respect to the beam trajectory is represented by straight poles centered around the average position of the trajectory in each pole (≈1cm from the axis), with the addition of simple shims to enlarge the width of the good field region. Of course, in order to be compatible with the present coils, the overall width of each pole must be reduced by ≈2cm. A structure of this kind, shown in Fig.13 has been simulated at CERN [20] with the magnet design

code TOSCA, validating the procedure by comparing the field obtained for the original design of the wiggler with the measured one. The position of the pole center has been chosen to minimize the contribution of the octupole term, while the shape of the shims has been determined by the optimization of its sensitivity to beam displacements.

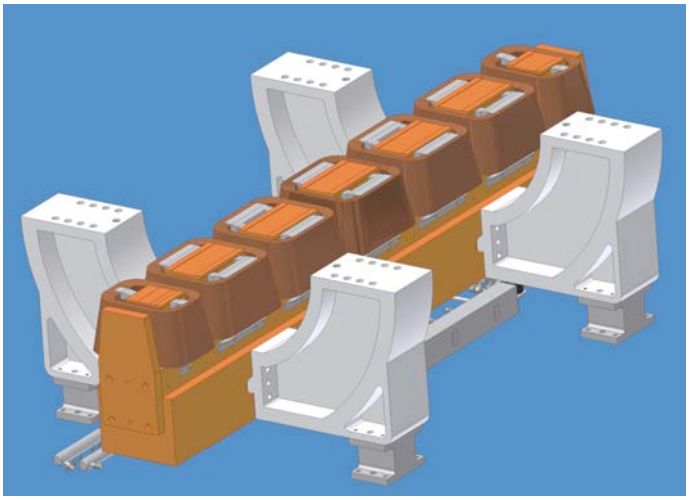

Fig. 13: View of the modified DAΦNE wiggler with alternated centering of the poles and shims.

The non linear contributions have been then compared to those obtained with the present wiggler, symmetric with respect to the magnet axis and displaced from the beam axis by half the oscillation amplitude of the beam inside the wiggler. Table II shows the results of the comparison: the sextupole term is reduced by a factor 2, the octupole by ≈35 and the decapole by ≈5.

Table II: Non linear terms in one full wiggler

	$\int \frac{\partial^2 B}{\partial x^2} ds (T/m)$	$\int \frac{\partial^3 B}{\partial x^3} ds (T/m^2)$	$\int \frac{\partial^4 B}{\partial x^4} ds (T/m^3)$
Present wiggler	-6.7	-838	41328
Modified wiggler	-3.3	-25	-7848

6. Beam pipe and hardware modifications

The beam pipe around the IP and in the two QD0s will be common to the two beams, and will start to bifurcate just before the QF1s, which must be very compact. The absence of the splitter magnets will avoid having large horizontal dispersion at the sextupole which will be used for the crabbed waist. The vacuum pipe will be also very simple. The two arc dipoles, leading to the short and long halves of the ring, will need a small magnetic field adjustment (B needs to be higher in the short arc dipole, lower in the long arc one). At present all the dipoles in both rings are connected in series and fed by a single power supply. This will have to be modified, and the power supplies of the present splitters will

be used to power these bends individually. All other IR magnets and power supplies will be reused except for the IP pm quadrupoles. Other elements just after the doublets (quadupoles, sextupoles and correctors) are those already in place; only their positions need to be rearranged. Most of the vacuum pipes and pumps will be reused, except for the IR ones. Fig. 14 shows a drawing of half of the modified IR1.

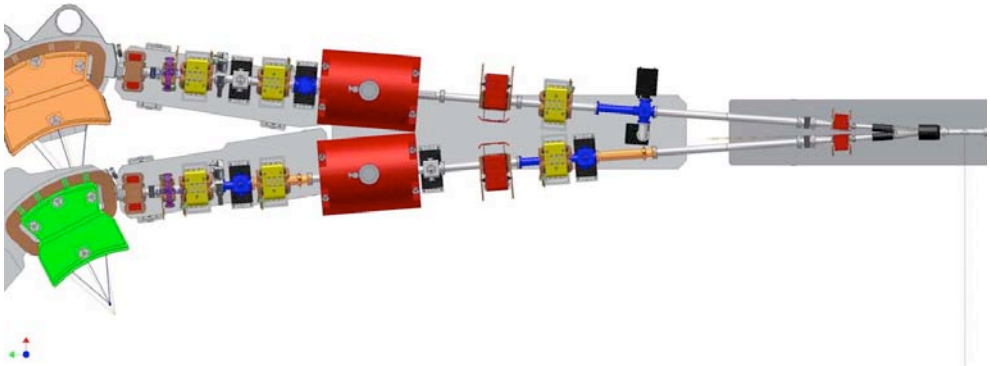

Fig. 14: View of the modified IR1 region (half).

Similar modifications will be made in the second IR (IR2), where the beams will not experience a low-beta insertion, and will be vertically separated in order to avoid collisions. A layout of half IR2 is presented in Fig. 15. A new design of the IP2 beam pipe, were the two lines will be vertically separated, is shown in Fig. 16.

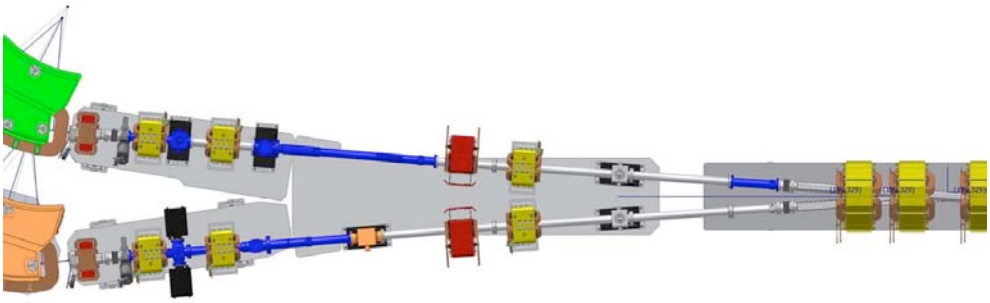

Fig. 15: View of the modified IR2 region (half).

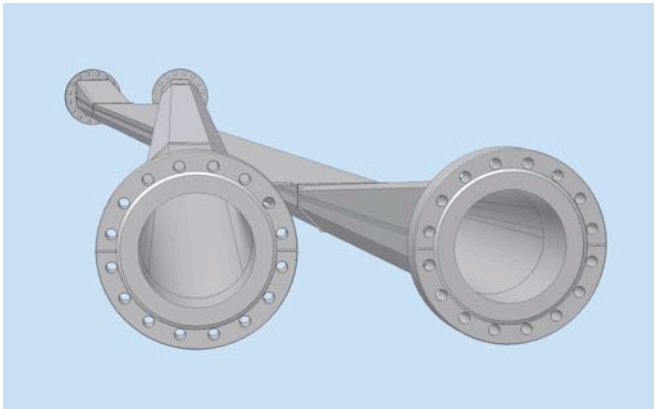

Fig. 16: View of the IP2 beam pipe.

7. Near IP Quadrupoles

The low-β section quadrupoles will be of the permanent magnet (PM) type. A set of two QD0 and four QF1 are required. A study of their characteristics has been performed, and a summary of their specifications [21] is given in Table III. Six permanent SmCo quadrupoles have been already designed with these characteristics. A close-up of the near IP region is shown in Fig. 17.

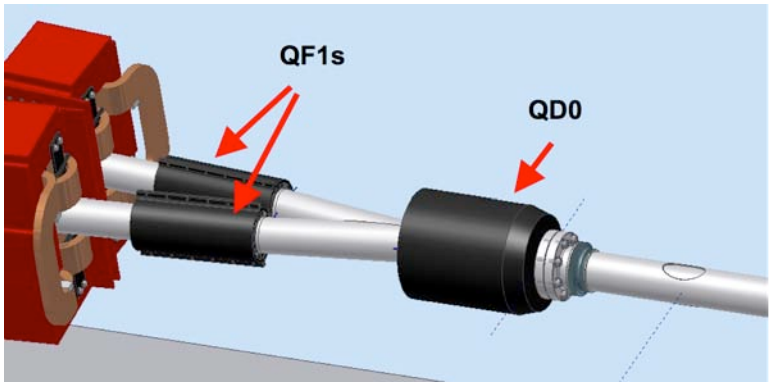

Fig. 17: Close up of the IP doublet.

Table III: Low-β PM quadrupoles preliminary specifications

Designation	**QD0**	**QF1**
Quantity	2	4
Minimun clear inside radius (mm)	33	30
PM inside radius (mm)	34	30,5
Maximum outside radius (mm)	100	45r/55ears/with cut
Magnetic length (mm)	230	240
REM physical length (mm)	230	240
Maximium mechanical length (mm)	240	250
Nominal gradient (T/m)	29.2	12.6
Integrated field strength (T)	6.7	3.
Good field region radius (mm)	20	20
Integrated field quality ldB/Bl	5,00E-04	5,00E-04
Maximum allowable mismatch of integrated gradient between magnets	1,00E-03	1,00E-03
REM stabilization temperature (°C)	150	150
Magnet material type	SmCo2:17	SmCo2:17
Magnet construction	2 half - split	2 half - split

8. Backgrounds

In the DAΦNE upgrade scheme the induced backgrounds will be dominated by Touschek scattering [22], as it is for the present configuration. Simulations of the Touschek effect with the crabbed waist optics have been performed using the same tool used for the KLOE run [23]: the reliability of this simulation code has been tested with the KLOE data, showing a good agreement [24].

Touschek scattering is a source of background due to the off-energy particles arising from the elastic scattering of particles within a bunch. Scattering results in two particles with energy errors $+\Delta p/p$ and $-\Delta p/p$ which follow betatron trajectories around the off-energy closed orbit. In the simulation Touschek particles are taken within one transversely Gaussian bunch with the proper energy spectra. Particles are tracked over many turns or until they are lost. In this way an estimate of the Touschek losses along the whole ring and at the IR is performed. Essentially all losses at the IR arise from the Touschek scattered particles in dispersive regions, so only these particles are simulated. Touschek scattered particles have a betatron oscillation which is proportional to the dispersion D, to the invariant H and to the momentum spread $\Delta p/p$:

$$x = \frac{\Delta p}{p}(|D| + \sqrt{H\beta})$$

The parameter H-invariant is defined by the following relation:

$$H = \gamma_x D_x^2 + 2\alpha_x D_x D_x' + \beta_x D_x'^2$$

Further details on the simulation can be found in [23], we summarize the results in the following. Fig. 18 shows the behaviour of the H function along the ring, starting from the IP: it appears that the value of H is almost equal for the four arcs and it is around 1.2, about a factor 2 lower with respect to the KLOE optics. The Touschek scattered particles perform large betatron oscillations in these four regions where H and D are high, with very similar energy spectra but different phase advance. The black curve in the right plot of Fig. 18 shows the Touschek probability density function for the constant H value region in arc PL1; for comparison also the KLOE optics case (red dotted line) is reported. The Touschek probability function is now higher, due to the lower emittance. This effect is only partly compensated by the lower values of H.

The trajectories of the Touschek particles and the location where they hit the beam pipe have been studied. The beam parameters used for these simulations are reported in Table I of section 3. Full tracking has been performed for one machine turn, and only particles with a relative energy deviation between 0.003 and 0.02 have been simulated, as particles with higher energy deviations get lost locally and do not contribute to backgrounds in the experiment, and particles with relative energy deviation < 0.003 are practically always kept inside the beam pipe.

The calculated trajectories of the particles scattered in the PL1 arc are shown together with the 15 σ_x curve (dotted green line) in Fig. 19. Similar analyses have been performed for the other three arcs. Longitudinal scraper positions along the ring have been checked together with their efficiency: as expected, the largest reduction of the IR losses associated with Touschek scattering is achieved by using the scraper closest to the IR: its optimized longitudinal position is found to be just after the focusing quadrupole QUAPL109 (s = -8.2 m in Fig. 19 and 21), corresponding to a maximum of β_x. The maximum opening of the scraper jaws should be up to 11 mm from the center of the beam pipe, corresponding to about ~8.5 σ_x (see Fig. 20). The scan of the calculated IR losses versus opening of internal and external jaws of IR scraper (SCHPL101) is reported in Fig. 20; the scrapers openings are measured from the center of the beam axis and expressed in number of σ_x. Losses are referred to Touschek particles generated in the PL1 arc only. Black dots are for the particles lost upstream the IP, red dots for the downstream ones. It appears that upstream rates vanish with the scraper at ~ 12 σ_x, downstream rates are minimized at ~ 8.5 σ_x.

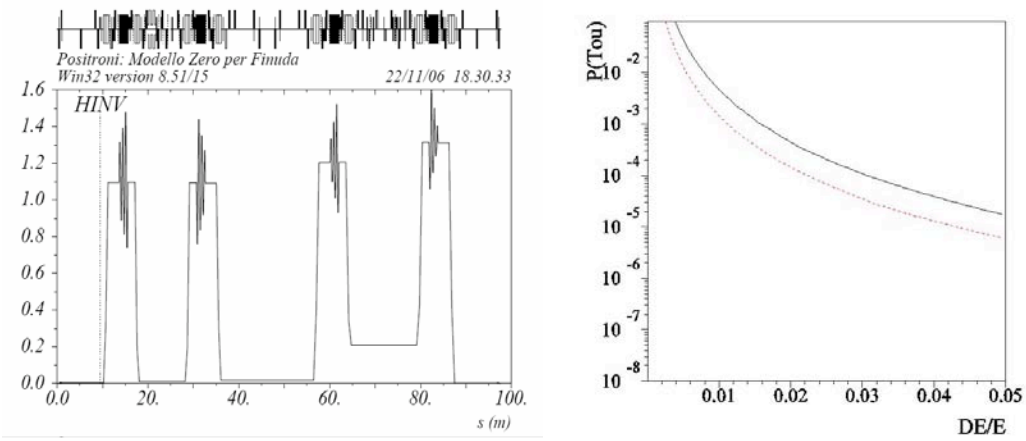

Fig. 18: Left: H function. Right: Touschek probability density function as a function of the energy deviation in arc PL1 (black curve) compared KLOE optics (red dotted line).

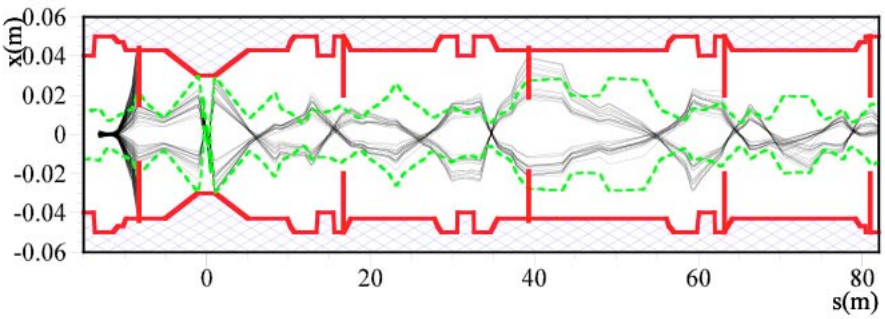

Fig. 19: Touschek particles trajectories scattered in PL1 and tracked for one machine turn, with only the IR scraper inserted. All the five available scrapers are shown. The dotted green curve represents 15σ_x of the beam. The IP is at s=0.

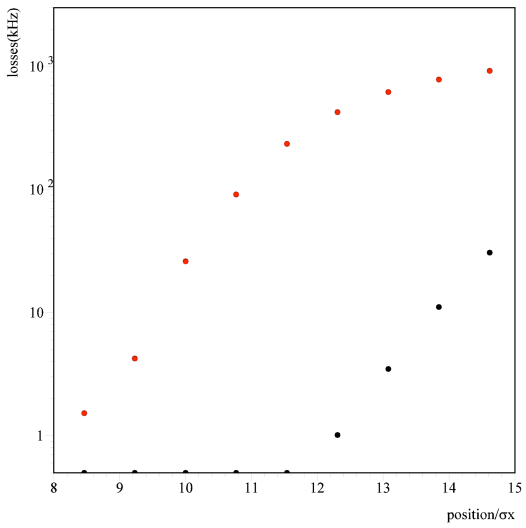

Fig. 20: IR losses coming from the arc upstream the IR as a function of the IR scraper openings measured in number of σ_x from the center of the beam axis. Black dots are losses upstream the IP, red dots are the downstream ones.

For each arc the losses at the IR have been investigated by calculating the scrapers efficiency. The contribution of each arc to the total and IR losses are summarized in Table IV. With this new optics most of the losses are concentrated in the IR, where the β_x function is high and the aperture small. As an example, Fig. 21 shows IR losses coming from arcs PL2 and PL1where scrapers are inserted. As shown in Table IV the scrapers are very efficient.

Contribution to IR losses from arc PS1 has been optimized by positioning SCHPS201 at S = - 46 m from the IP, corresponding to large radial oscillations of scattered particles (see Fig. 22). A masking system between the pipe and the low-β quadrupoles will be incorporated to shield the detector from beam-generated background.

Table IV: Lost particles per bunch per beam with a beam current of 13mA.

	Total losses [KHz] No scrapers	IR losses [KHz] No scrapers	IR losses [KHz] With scrapers	Effective scraper
PL1	$1.91 \cdot 10^3$	$1.91 \cdot 10^3$	1.52	SCHPL101 = 8.5 σ_x
PL2	$7.63 \cdot 10^3$	$5.41 \cdot 10^3$	1.82	SCHPL101 = 8.5 σ_x ; SCHPL110 = 18 σ_x
PS2	$2.40 \cdot 10^3$	$1.64 \cdot 10^3$	0	SCHPL101 = 8.5 σ_x ; SCHPS201 = 13 σ_x
PS1	$2.15 \cdot 10^3$	$1.52 \cdot 10^3$	0	SCHPL101 = 8.5 σ_x ; SCHPS101 = 14.4 σ_x
Tot.	$14.09 \cdot 10^3$	$10.48 \cdot 10^3$	3.34	

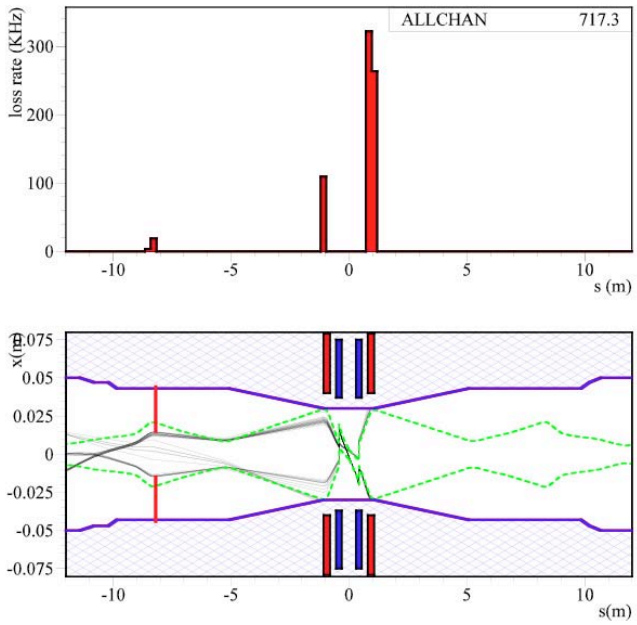

Fig. 21: Distribution (upper) and trajectories (lower) of Touschek particles lost at the IR, in dotted green is the15σ_x beam envelope (IP = 0).

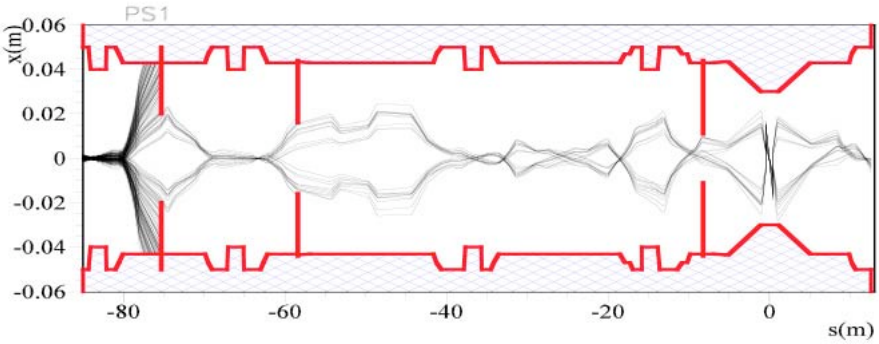

Fig. 22: Touschek particles trajectories scattered in PS1and tracked for one machine turn with scrapers inserted (IP = 0)..

In conclusion, we can say that particle losses due to Touschek effect are expected to be quite high with the Siddharta optics, if compared to the KLOE one in the standard running conditions. Losses are essentially concentrated at the IR where the physical aperture is small; however scrapers are expected to be very efficient.

9. Beam Impedance calculations

The beam coupling impedance should not be a problem for the crabbed waist experiment. After the vacuum chamber modifications we expect to have even smaller impedance with respect to that in present operating conditions [25]. The impedance

reduction comes mainly from the installation of the new injection kickers having a reduced beam impedance and to the simplified design of both IR vacuum chambers, that are essentially straight tubes without sharp discontinuities.

However, attention has been paid in designing the Y-shape vacuum chamber section, where the common IR chamber is split in the two separate rings. The principal problem that may arise is an excessive power loss due to beam interaction with higher order modes (HOM) trapped in the Y-section. Indeed, according to SLAC experience, the power loss in the Y-shaped chamber of the PEP-II collider has been measured to be of the order of several kW [26].

In order to calculate the loss factor and to evaluate the contribution of the section to the machine broad-band impedance we have performed simulations with MAFIA and GdiFidl numerical codes. The calculated loss factor is 5.77×10^9 V/C that would give about 80 W of power losses for 110 bunches with a current of 20 mA per bunch and a bunch length of 2 cm. The contribution of the Y-chamber to the low frequency impedance is estimated to be 13 mΩ, about 2% of the total ring impedance budget.

These numbers do not represent any danger for the collider performance. However, the above estimates have been done in "single pass" approximation, i.e. without taking into account possible power loss enhancement due to long-range wake fields. Time domain simulations with MAFIA indicated the presence of HOMs in the Y-chambers (see the long lasting wakes behind the bunch in Fig. 23). In order to evaluate parameters of the potentially dangerous HOMs an intensive study in the frequency domain has been carried out with the HFSS code.

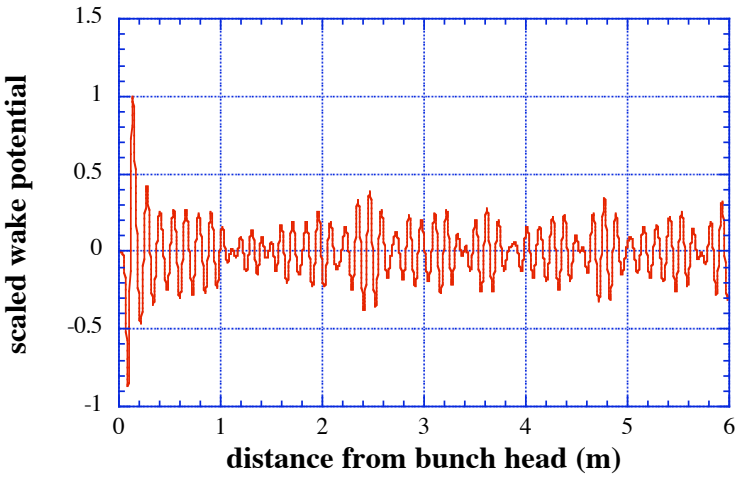

Fig. 23: Wake potential as computed by MAFIA.

The strongest mode found has the frequency close to the first TE waveguide mode cut-off, f = 2.678 GHz. The mode distribution is shown in Fig. 24. Despite the HOM electric field is directed horizontally it still contributes to the power losses since the beam trajectory is not symmetric with respect to the vacuum chamber axis. The shunt impedance of the mode evaluated along the beam pass is 118 Ω, while its quality factor is 17800.

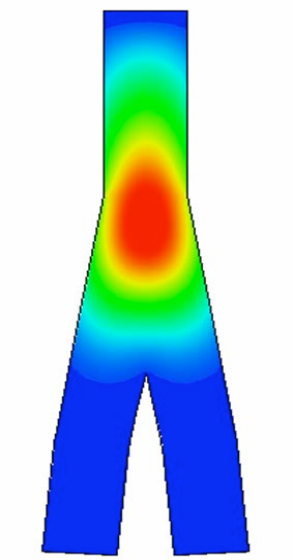

Fig. 24: Mode distribution for first TE waveguide mode cut-off, f = 2.678 GHz.

In the worst possible scenario, when one of the powerful beam spectrum lines (at RF frequency harmonics) is in full coupling with this mode, the lost power would not exceed 200 W. Despite such a power seems to be manageable, we still decided to place cooling channels at the Y-chamber junction as shown in Fig. 25. This additional cooling will play a double role: to eliminate heating due to the HOM, if necessary, and to shift the mode frequency with respect to the dangerous power spectrum lines, thus reducing the heating itself.

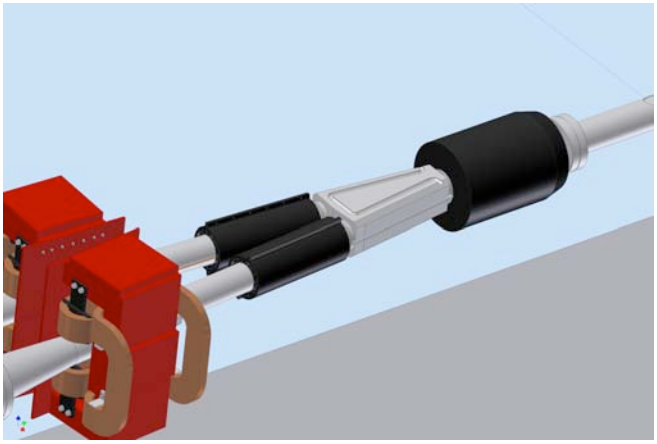

Fig. 25: Y-chamber junction.

10. Injection system upgrade

The present DAΦNE injection system is based on magnetic kickers [27]. The possibility of a new injection system based on fast stripline kickers has been taken into account after studies made for the ILC Damping Rings [28]. While in the present DAΦNE

injection kickers the deflection is given by the magnetic field generated by current flowing in two coils, in the stripline kickers the deflection is given by both the magnetic and the electric fields of a TEM wave travelling in the structure (see Fig. 26). The deflecting wave generated by two fast high voltage (HV) pulsers with opposite polarity travels into the structure at the velocity of light and is absorbed on an external load. Details on the design of the new injection kickers can be found in [29]. Compared to the present DAΦNE injection kickers the new ones have these characteristics:

a) much shorter pulse (≈12 ns instead of ≈150 ns);
b) better uniformity of the deflecting field;
c) lower impedance;
d) possibility of higher injection rate (max 50 Hz).

The much shorter pulse length allows perturbing only the injected bunch and the two adjacent ones while, at present, a large fraction of the stored bunches (50 over 110, with 2.7 ns bunch spacing) are affected by the injection kick. This improvement can increase the current threshold of the transverse instability in the positron ring (as it has already been observed experimentally at DAΦNE). The better uniformity of the deflecting field can also increase the injection efficiency at high currents and reduce the background to the detectors during injection. The broadband impedance, according to the calculations, is reduced by a factor 3 with respect to the present kickers. Moreover, since the new kickers have been designed with a beam pipe cross section similar to that of the dipoles and septum regions, reduced taper transitions are needed between the different sections and this also contributes to the reduction of the machine impedance. Finally, the possibility of injection at 50 Hz can be useful for future upgrades of the whole injection system.

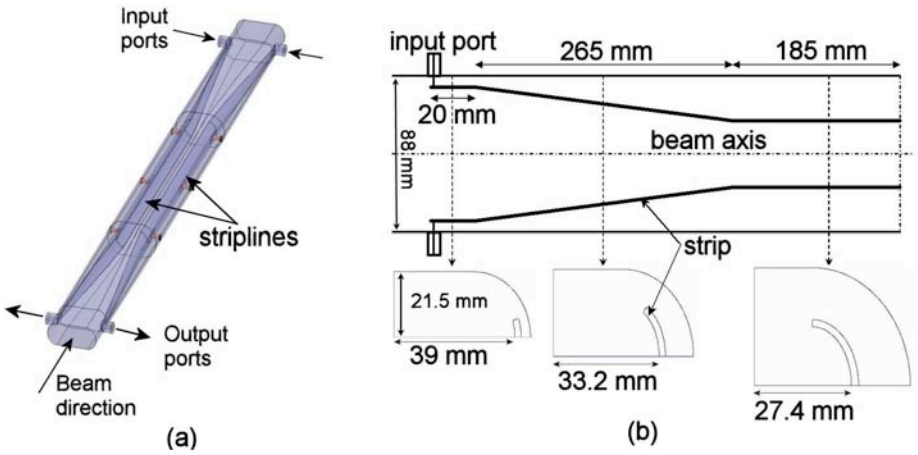

Fig. 26: (a) 3D model of the structure; (b) sketch of half kicker structure with cross sections at different longitudinal positions.

The injection system upgrade will consist of three different but related parts: new kicker structures, HV input pulse generators and new vacuum chamber between dipole regions and kicker ones.

The design of the kickers is based on a tapered strip with rectangular vacuum chamber cross section in order to simultaneously:

a) improve the deflecting field quality obtaining a uniform transverse deflection as a function of the transverse coordinate (horizontal in particular);
b) reduce the beam coupling impedance because of the tapered transition between the beam pipe and the kicker structure;
c) have a uniform beam pipe cross section between the dipole region (that has a rectangular cross section) and the kickers region. This also reduces the total beam coupling impedance of the machine;
d) obtain a better matching between the generator and the kicker structure at high frequency. This can avoid multiple reflections of the deflecting pulse in the kicker structure that can perturb the stored bunches. Moreover it can allow extracting all the power released to the HOM of the structure by the beam.

The mechanical drawing of the kicker is shown in Fig. 27. The required voltage per strip to reach the desired bunch deflection is ≈ 45 kV. The HV pulse requirements are summarized in Table V referring to the quantities sketched in Fig. 28.

Fig. 27: Mechanical drawing of the kicker.

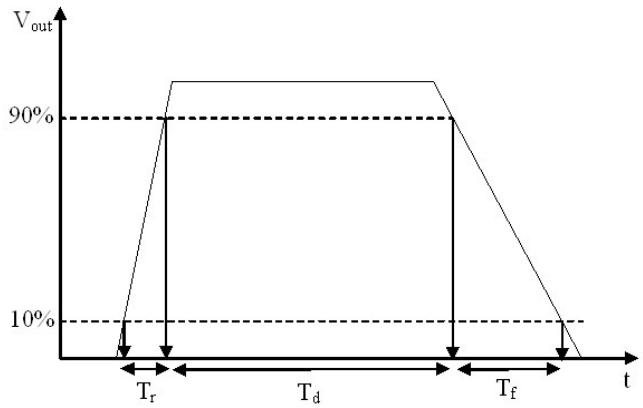

Fig. 28: HV input pulse sketch.

Table V: HV input pulse technical specifications

Max repetition rate [Hz]	50
Max output voltage [kV]	50
Output voltage duration T_d (90%-90%) [ns]	5.5 ± 0.1
Rise time and fall time sum T_r+T_f [ns]	2 ± 0.1
Pulse jitter [ps]	50 ± 20
Load impedance [Ω]	50

11. Luminosity monitor

DAΦNE luminosity can be determined by counting Bhabha events at small angle, or by counting single bremmstrahlung events on one of the two detector sides. We intend to perform luminosity measurement using both methods.

Two counters with proper azimuthal segmentation positioned just around the QD0s can provide a coincidence signal for elastic scattering (Bhabha) events. Depending upon the angular acceptance of the counters, counting rates up to several kHz can be obtained at the design luminosity. Because of momentum conservation, the two scattered particles are emitted at a fixed relative angle, which helps in minimizing contamination from other two-body processes. Thus, ideally, the Bhabha detector can be built using simple counting devices. However, it might be necessary to use a calorimetric technique, in order to reject the possible background due to beam related accidentals.

In single bremmstrahlung events the electrons (positrons), which have emitted a photon of given energy, are scattered off the beam line at a position which depends on their residual energy and on the actual magnetic fields they see along their flight path. According to preliminary MAD calculations, electrons in the range 100-230 MeV energy will leave the beam pipe in the zone between the QD0 and QF1s. Counting rates as high as several MHz are expected for luminosities exceeding 10^{32} $cm^{-2}s^{-1}$. We intend to install a counting device of the type which is being developed as tagger for two-photon events for the KLOE-2 experiment. It consists of a series of silicon strips, to detect the electrons, followed by scintillators for triggering purposes. The energy of the scattered electron is reconstructed by the knowledge of the strip which has actually fired. Again, the most relevant problem is to fight the machine related background, which has to be evaluated and eventually subtracted in single beam runs.

It is worthwhile to note that, being the two methods totally uncorrelated, they could provide useful reciprocal indications of the level of background of the two measurements.

12. Cost estimate

The estimated cost for the upgrades is shown in Table VI. The cost of PM quads and kickers is relatively accurate, since the figures from the vendors are already available. The other components are estimated from projections of similar elements acquired in the past.

Table VI: Cost estimate

	Kilo-Euros
PM quads	350
Vacuum chambers, valves, pumps	150*
Pulsed Kickers	340*
New wigglers poles	225
Modifications to electrical/hydraulic/mechanical plants	60
External labor	60
Contingency	100
Total	**1285+VAT**

*50% of this amount has been already funded by INFN-NTA_ILC in 2006.

13. Conclusions

A new IR for the Siddharta detector, compatible with the large crossing angle option, is feasible. The predicted large luminosity boost is based both on geometric and beam dynamics considerations, fully supported by extensive beam-beam simulations. Six times more luminosity for a given current leads to a ten times better luminosity/background ratio.

Top-of-the-line accelerator physics should be at reach during the Siddharta run, and very small vertical sizes should be reached, amongst the smallest achieved worldwide. ILC-like kickers, new wigglers design and TiN coating will help to give further leading-edge accelerator physics.

References

[1] P. Raimondi, "Status of SuperB Effort", 2nd SuperB Workshop, LNF, Frascati, March 2006, http://www.lnf.infn.it/conference/superb06/talks/raimondi1.ppt

[2] A. Gallo et al., "DAΦNE status report", Proc. of EPAC 2006, Edimburgh, Scotland, pp. 606-608.

[3] P. Raimondi, M. Zobov, DAΦNE Techn. Note G-58, April 2003; D. Shatilov, M. Zobov, ICFA Beam Dynamics Newsletter 37:99-109, 2005.

[4] K. Hirata, "Analysis of beam-beam interactions with a large crossing angle", Phys. Rev. Lett. 74:2228-2231, 1995.

[5] F. Zimmerman, F. Ruggiero, "Luminosity optimization near the beam-beam limit by increasing bunch length or crossing angle, Phys. Rev. ST Accel. Beams 5:061001, 2002.

[6] D.V. Pestrikov, "Vertical Synchrobetatron Resonances due to Beam-Beam Interaction with Horizontal Crossing", Nucl. Instrum. Meth. A336:427-437, 1993.

[7] J. Seeman et al., "Parameters of a Super-B-Factory Design", Proceedings of 2005 Particle Accelerator Conference, pp. 2333-2335, 2005.

[8] H. Koiso, "Super B-Factories", Proc. of 2005 Particle Accelerator Conference, Knoxville, USA, pp. 64-68, 2005.
[9] "DANAE LoI", http://www.lnf.infn.it/lnfadmin/direzione/roadmap/DANAE_LOI.pdf
[10] K. Ohmi et al., "Luminosity Limit due to the Beam-Beam Interactions with or without Crossing Angle", Phys. Rev. ST Accel. Beams 7:104401, 2004.
[11] P. Raimondi, D. Shatilov and M Zobov, "Beam-Beam Issues for Colliding Schemes with Large Piwinski Angle and Crabbed Waist", in preparation.
[12] D. Shatilov, M. Zobov, "Tune Shift in Beam-Beam Collisions with an Arbitrary Crossing Angle", DAΦNE Techn. Note G-59, 2003.
[13] K. Hirata, "BBC User's Guide: A Computer Code for Beam-Beam Interactions with a Crossing Angle, Version 3.4", CERN SL-Note-97-57-AP, Aug. 1997.
[14] A. Drago, private communication.
[15] D. Alesini et al., "Fast Injection Kicker for DAΦNE and ILC Damping Rings", DAΦNE Techn. Note I-17, 2006.
[16] "KEKB B-Factory Design Report", KEK Report 95-7, Aug. 1995.
[17] K. Hirata, D. Shatilov and M. Zobov, "Beam-Beam Interaction Study for DAΦNE", Frascati Phys. Ser. 10: 303-308, 1998.
[18] Mini Workshop on "Wiggler Optimization for Emittance Control", Frascati, Feb. 2005, unpublished.
[19] A. Battisti et al. "The modified wiggler of the DAΦNE Main Rings", DAΦNE Techn. Note MM-34, 2004.
[20] S. Bettoni – PhD Thesis – in preparation.
[21] C. Sanelli, private communication.
[22] C. Bernardini, G. F. Corazza, G. Di Giugno, G. Ghigo, J. Haissinski, P. Marin, R. Querzoli and B. Touschek., Phys. Rev. Lett., vol. 10, 1963, p. 407.
[23] M. Boscolo, M. Antonelli, S. Guiducci, "Simulations and measurements of the Touschek background at DAΦNE", EPAC02, Paris, France, 2002.
[24] M. Boscolo, S. Guiducci, "A Comparison between data and simulations of the DAΦNE beam induced backgrounds in KLOE", DAΦNE Techn. Note IR-10, 2001.
[25] M. Zobov et. al, DAΦNE Technical Note B-3, 1998.
[26] A. Novokhatskii, presentation at the 3rd SuperB Workshop, SLAC, June 2006, http://www-conf.slac.stanford.edu/superb/
[27] S. De Simone and A. Ghigo, "DAΦNE Accumulator Kickers", EPAC 92, Berlin, Germasny, March 1992.
[28] A. Woslki, J. Gao, S. Guiducci editors, "Configuration Studies and Recommendations for the ILC Damping Rings", LBNL–59449, Cockroft–06–04, Feb. 2006, available at: http://www.desy.de/~awolski/ILCDR/DRConfigurationStudy_files/DRConfigRecommend.pdf
[29] D. Alesini, F. Marcellini, S. Guiducci, P Raimondi, "Fast injection kickers for DAΦNE and ILC damping rings", DAΦNE Tech. Note I-17, 2006.